Emission redshift in DCM2-doped Alq_3 caused by nonlinear Stark shifts and Förster-mediated exciton diffusion

Graziâni Candiotto,[1,2,*,†] Ronaldo Giro,[3,*,‡] Bruno A. C. Horta,[2] Flávia P. Rosselli,[4,5] Marcelo de Cicco,[4] Carlos A. Achete,[4] Marco Cremona,[4,6] and Rodrigo B. Capaz[1,4,§]

[1]*Instituto de Física, Universidade Federal do Rio de Janeiro, Rio de Janeiro, Rio de Janeiro 21941-972, Brazil*
[2]*Instituto de Química, Universidade Federal do Rio de Janeiro, Rio de Janeiro, Rio de Janeiro 21941-909, Brazil*
[3]*IBM Research, Avenida Pasteur 138/146, Rio de Janeiro, Rio de Janeiro 22290-240, Brazil*
[4]*Instituto Nacional de Metrologia, Qualidade e Tecnologia, Duque de Caxias, Rio de Janeiro 25250-020, Brazil*
[5]*Departamento de Química, Universidade Federal de São Carlos, São Carlos, São Paulo 13565-905, Brazil*
[6]*LOEM, Departamento de Física, Pontifícia Universidade Católica do Rio de Janeiro, Rio de Janeiro, Rio de Janeiro 22451-900, Brazil*

(Received 1 June 2020; accepted 6 November 2020; published 1 December 2020)

Organic light-emitting diode (OLED) devices in the archetype small-molecule fluorescent guest-host system tris(8-hydroxyquinolinato) aluminum (Alq_3) doped with 4-(dicyanomethylene)-2-methyl-6-julolidyl-9-enyl-4H-pyran (DCM2) displays a redshift in light-emission frequency which is extremely sensitive to the dopant concentration. This effect can be used to tune the emission frequency in this particular class of OLEDs. In this work, a model is proposed to describe this effect using a combination of density functional theory quantum-chemical calculations and stochastic simulations of exciton diffusion via a Förster mechanism. The results show that the permanent dipole moments of the Alq_3 molecules generate random electric fields that are large enough to cause a nonlinear Stark shift in the band gap of neighboring DCM2 molecules. As a consequence of these nonlinear shifts, a non-Gaussian probability distribution of highest occupied molecular orbital to lowest unoccupied molecular orbital (HOMO-LUMO) gaps for the DCM2 molecules in the Alq_3 matrix is observed, with long exponential tails to the low-energy side. Surprisingly, this probability distribution of DCM2 HOMO-LUMO gaps is virtually independent of DCM2 concentration into the Alq_3 matrix, at least up to a fraction of 10%. This study shows that this distribution of gaps, combined with out-of-equilibrium exciton diffusion among DCM2 molecules, is sufficient to explain the experimentally observed emission redshift.

DOI: 10.1103/PhysRevB.102.235401

I. INTRODUCTION

Organic light-emitting diodes (OLEDs) are a relatively new class of devices already used for display technologies [1,2] (TVs, computers, cell phones, palmtop computer screens, etc.) [3,4] and other applications as an illumination source [5], lasers [6–8], and medical devices [9]. The great interest in this technology is related to the low cost of organic materials, the simplicity of organic thin-film growth, the ease of integrability with conventional technology, and the versatility of carbon chemistry, among other advantages. However, this technology has some drawbacks, as the device lifetime still needs to be improved and OLEDs show generally a broad electroluminescence (EL), resulting in unsaturated emission colors.

In order to overcome the latter problem, Bulović *et al.* [10,11] developed OLED devices by doping a "host" material, aluminum tris(8-hydroxy quinoline) [Alq_3; Fig. 1(a)] [12], with "guest" molecules, [2-methyl-6-[2-(2,3,6,7-tetrahydro-1H, 5H-benzo[i,j] quinolizin-9-yl)-ethenyl]-4H-pyran-4-ylidene] propane-dinitrile [DCM2; Fig. 1(b)] [12], hereafter referred to as Alq_3:DCM2. In these devices, excitons are generated in the Alq_3 molecules and efficiently transferred by Förster resonance energy transfer (FRET) [7,13,14] to the DCM2 molecules. Moreover, these devices show saturated color emission [15], and the color can vary from yellow to red as the concentration of guest (DCM2) molecules is increased from 1% to 10%. This redshift amounts to roughly 50 nm, with a relatively unchanged peak width over this range of doping [6,10,11]. Due to its interesting properties and numerous applications in the area of organic thin films, the Alq_3:DCM2 system is still a relevant topic which draws the attention of the scientific community [7,16,17].

Previous works suggested that the spectral shift was due to excimer formation [11,18] or hydrogen bonds in solution [19]. Bulović *et al.* [10,11] challenged these interpretations because excimer formation would not result in a rigid and continuous shift of the EL spectrum. In addition, hydrogen bonds with DCM2 molecules are not possible in solution [10,11]. The similarity of the spectral widths and magnitudes of the peak shifts of the spectra both in solution and in thin films suggested to Bulović *et al.* [10,11] to attribute the redshift in energy due to the polarization induced by DCM2 molecules. In their own words, "as the DCM2

*These authors contributed equally to this work.
†gcandiotto@iq.ufrj.br
‡rgiro@br.ibm.com
§capaz@if.ufrj.br

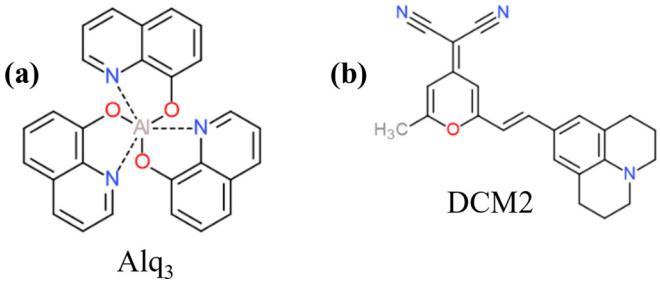

FIG. 1. Schematic representation of (a) Alq_3 and (b) DCM2 molecules.

concentration in the relatively non-polar Alq_3 is increased, the distance between nearest neighbor, highly polar, DCM2 molecules decreases, thereby increasing the local polarization field. This polarization tends to redshift the DCM2 emission spectrum" [10,11].

In a series of articles [10,11,20], Bulović and collaborators called this the solid-state solvation effect (SSSE), in analogy to the "solvation effect" of organic dyes in liquid solutions, which is observed when the dye absorption and emission spectra are influenced by dipole moment of the surrounding solvent molecules [21]. The solvation effect results from intermolecular solute-solvent interaction forces such as dipole-dipole and dipole-induced dipole (these interactions tend to alter the energy difference between the ground and excited states of the solute). The SSSE effect has been used for tuning the luminescent emission spectrum of dipolar molecules by adjusting the strength of intermolecular dipole-dipole interactions using a doped guest-host molecular organic thin-film system [11,20].

Bulović *et al.* [10,11] also made an important observation: Since the molecules in the solid solution must be randomly distributed, over a large volume, the net DCM2 dipole moment averages to zero. However, considering that the dipole field decreases as $1/r^3$, where r is the distance between dipoles, near any given radiating molecule there should be a net local electric field due to the dipole moments of neighboring DCM2 molecules which, on average, influences the spectral emission.

Other models have been suggested [11,22] to explain the observed redshift. In 2001, Baldo *et al.* [22] introduced the so-called local order theory. This theory is based on the formation of aggregates of guest molecules in the host matrix. Baldo *et al.* argued that as the DCM2 concentration increases from 1% to 10%, the DCM2 molecules readily aggregate. The spectral shifts are then explained due to the high electric fields associated with local ordering of the polar DCM2 molecules in aggregate domains. In a following work, Madigan and Bulović [11] developed a model of solvatochromism relating the experimentally observed changes in emission and absorption spectra of a solute to the electronic permittivity of a solvent. This model does not require the assumption of aggregation of DCM2 to explain the redshift, and it was supported by experimental data [11].

Regardless of whether the spectral redshift is related to aggregation or not, all previous models relied on the fact that emission spectra would vary with changes in local electric field due to high electric dipole moment and dielectric constant of DCM2, as its concentration increases from 1% to 10%. However, the detailed mechanism for this effect was not investigated at the level of quantum-chemical calculations. In particular, the association of a strong emission redshift with an electric field acting on the DMC2 molecules is puzzling since changes in the electronic or optical gap under an electric field (Stark shifts) are typically linear to first order. Therefore, a randomly oriented field should, in principle, give rise to both positive and negative variations of the gap, with a nearly zero net effect.

In the present work, we develop a model to explain the redshift emission in DCM2-doped Alq_3, supported by a combination of density functional theory (DFT) quantum-chemical calculations and stochastic simulations of exciton diffusion and emission. Surprisingly, the energy gap distribution of DCM2 molecules under a random distribution of DCM2 and Alq_3 dipoles is rather independent of the DCM2 concentrations (for up to 10% DCM2), as just the smaller dipole moments of neighboring Alq_3 molecules are sufficient to produce the necessary gap variations in DCM2 to account for the observed redshift. Moreover, the calculated Stark shifts are highly nonlinear, producing a probability distribution of DCM2 gaps with a long tail to the low-energy side. Finally, the observed concentration dependence of the redshift is explained by exciton diffusion via the FRET mechanism.

This paper is organized as follows: Sec. II describes quantum-chemical calculations of the highest-occupied molecular orbital to lowest-unoccupied molecular orbital (HOMO-LUMO) gap variations of DCM2 under electric fields (Stark shift). Section III presents simulations of the local electric field on DCM2 and the determination of the gap distribution using random Alq_3 and DCM2 dipoles distribution. Section IV describes the kinetic Monte Carlo (kMC) simulations of exciton diffusion and emission via Föster energy transfer. Finally, Sec. V presents the main conclusions of the present work.

II. STARK SHIFT

A. Methodology

Since the random distribution of dipole moments of Alq_3 and DCM2 molecules results in an effective electric field acting on the DCM2 dopant molecules, initially, we established the dependence of the DCM2 HOMO-LUMO gap as a function of the intensity and orientation of this field; that is, the Stark shift is evaluated. To establish this dependence and at the same time ensure that our approach has quantitative and predictive capabilities, the molecular geometry, dipole moment, polarizability tensor, and HOMO-LUMO gap must be calculated using *ab initio* methods. The quantum-chemical calculations were performed using the GAUSSIAN03 program [23]. For the optimization of the geometry, dipole moment, and polarizability tensor of DCM2 and Alq_3 molecules, the generalized-gradient-approximation (GGA) exchangecorrelation functionals of Perdew, Burke, and Ernzerhof (PBE1PBE) [24–26] was used, along with a split-valence double-zeta polarized based in Gaussian type orbitals (6-31G (d, p)) [27] basis set.

Once the geometry of the DCM2 molecular structure was optimized [see Fig. 2(a)], electric fields $\vec{E}$ of various

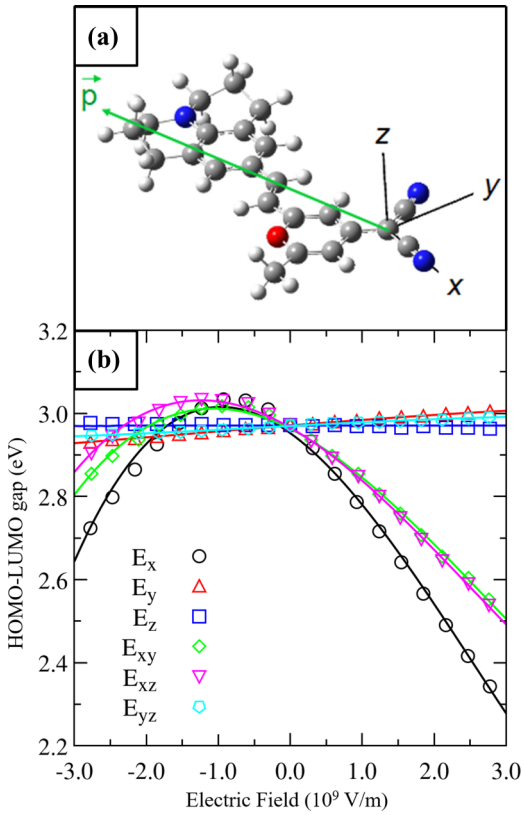

FIG. 2. (a) Optimized geometry of the DCM2 molecule. Almost all the atoms of the DCM2 molecule are lying in the xy plane. Gray, white, blue, and red spheres represent carbon, hydrogen, nitrogen, and oxygen atoms, respectively. The arrow shows the orientation of the dipole moment. The calculated DCM2 dipole moment vector is $\vec{p}_p = -12.6\hat{x} - 6.9\hat{y} - 0.2\hat{z}$ D. (b) DCM2 HOMO-LUMO gap as a function of applied electric field along directions x, y, and z. Solid lines represent the respective fit for each direction of the electrical field. Notice that the x component shows a stronger and nonlinear dependence on the gap. The x direction is almost parallel to the DCM2 dipole moment.

intensities were applied in different orientations with respect to DCM2 molecules [see Fig. 2(b)]. For these calculations, six different directions were chosen (E_x, E_y, E_z, E_{xy}, E_{yz}, and E_{xz}): parallel to the x, y, and z axes, at a 45° angle with respect to the x axis in the xy plane, at a 45° angle with respect to the y axis in the yz plane, and, finally, at a 45° angle with respect to the z axis in the xz plane. For this study, we performed self-consistent field (SCF) calculations using GAUSSIAN03 [23] within DFT. In this case the Becke three-parameter Lee-Yang-Parr (B3LYP) [28–31] hybrid functional was used for the exchange-correlation term in DFT, with the same base set as in the geometry optimization. The SCF calculations for this case are justified because it is expected that, in a solid-state film, DCM2 molecules in the Alq$_3$ matrix do not have enough space to accommodate geometry relaxation.

B. Results

Based on the *ab initio* DFT approach described previously, we first calculate the dipole moment and the polarizability tensor of Alq$_3$ and DCM2 molecules. These properties will be used in Sec. III. As expected, DCM2 molecules are highly polar, with a ground state dipole moment of 14.4 D, compared to the Alq$_3$ dipole moment of 4.4 D. These values are in good agreement with those reported in the literature [20,32]. In Fig. 2(a) we show the optimized DCM2 geometry and the dipole moment vector. As one can see, the dipole moment is oriented from the two carbon-nitrogen groups towards the oxygen atom. This is due to the balance of electronic charge between the oxygen (negative) and the two carbon-nitrogen groups (positive) at the ends of the DCM2 molecule.

Figure 2(b) shows the dependence of the DCM2 HOMO-LUMO gap as a function of the electric field (Stark effect). The Stark effect is stronger when the electric field is applied parallel to the x direction (E_x is the electric field in the x direction). In this case, this effect has a nonlinear dependence. We also show the dependence of the DCM2 gap regarding variations of the applied electric field in other directions. For the E_y, E_z, and E_{yz} directions there is almost no variation of DCM2 gaps with respect to the electric field, but for E_{xy} and E_{xz} directions a behavior similar to that in the E_x direction is observed.

Due to the nonlinear behavior shown in Fig. 2(b), an analytical expression for the HOMO-LUMO gap of DMC2 E_g as a function of the electric field needs to consider up to quadratic terms:

$$\begin{aligned} E_g(\vec{E}) &= E_g(0) + \vec{\alpha}\cdot\vec{E} + \vec{E}^t\cdot\boldsymbol{\beta}\cdot\vec{E} \\ &= E_g(0) + \alpha_x E_x + \alpha_y E_y + \alpha_z E_z + \beta_{xx}E_x^2 + \beta_{yy}E_y^2 \\ &\quad + \beta_{zz}E_z^2 + 2\beta_{xy}E_xE_y + 2\beta_{xz}E_xE_z + 2\beta_{yz}E_yE_z, \quad (1) \end{aligned}$$

where $E_g(0) = 2.96$ eV is the HOMO-LUMO gap for the ground state at zero electric field. The coefficients α_i and β_{ij} are obtained by fitting the DCM2 HOMO-LUMO gap dependence for each direction of the applied electric field shown in Fig. 2(b) by quadratic polynomials. The resulting values of α_i and β_{ij} are shown in Table I.

TABLE I. Values of the α_i and β_{ij} terms from Eq. (1). These values are obtained from the coefficients of polynomial fitting from the DCM2 gap dependence of the applied electric field [see Fig. 2(b)].

Direction $\hat{\imath}$	α_i [eV (V/m)]	β_{ij} [eV (V/m)^2]
$\hat{x}$	-1.24800×10^{-10}	-5.46220×10^{-20}
$\hat{y}$	1.32409×10^{-11}	-3.89083×10^{-22}
$\hat{z}$	-1.76392×10^{-12}	-7.73069×10^{-23}
$\hat{x}+\hat{y}$		-3.42360×10^{-20}
$\hat{x}+\hat{z}$		-3.22504×10^{-20}
$\hat{y}+\hat{z}$		-1.59986×10^{-22}

III. ELECTRIC FIELD AND ENERGY GAP DISTRIBUTIONS

In this section, the resulting electric field at each DCM2 molecule caused by a random distribution of Alq$_3$ and DCM2 dipole moments is calculated. Once this electric field is obtained, the DCM2 gap shift is calculated using Eq. (1). With this procedure it is possible to obtain the histogram of the

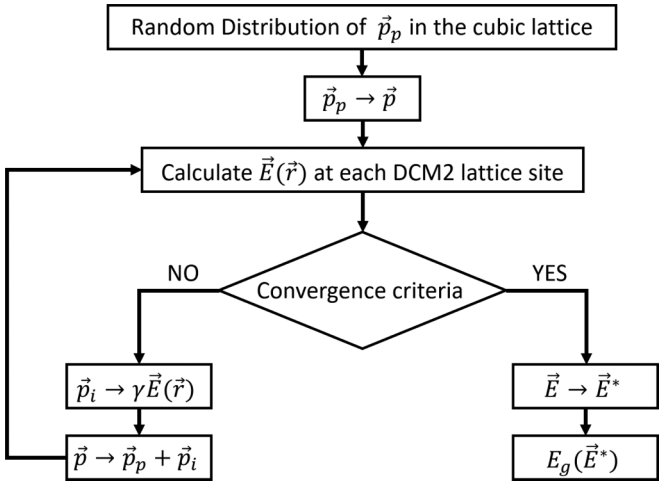

FIG. 3. Flowchart illustrating the self-consistent procedure used in this work to calculate the DCM2 energy gap distribution due to the random electric field generated by the Alq_3 and DCM2 permanent and induced dipoles. $\vec{p}$, $\vec{p}_p$, and $\vec{p}_i$ indicate the total, permanent, and induced dipole moments of each molecule, γ is the polarizability tensor, $\vec{E}$ is the local electric field, and $\vec{E}^*$ represents its converged value.

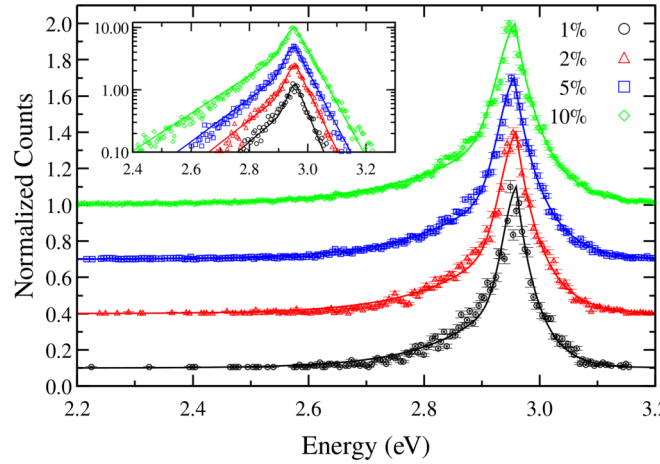

FIG. 4. HOMO-LUMO gap distribution for different DCM2 concentrations. Points represent the histogram of the DCM2 gap, and lines show the fitted gap distribution function. In the inset, the HOMO-LUMO gap distributions are represented on a logarithmic scale. Different curves represent various DCM2 concentration in the Alq_3 matrix, and they are displaced vertically for clarity. Solid lines represent the respective fit for each DCM2 concentration.

DCM2 gap distribution for each concentration of DCM2 molecules into the Alq_3 matrix.

To calculate the resulting electric field in each of the DCM2 molecules, we consider not only the permanent dipole moments of Alq_3 and DCM2 molecules but also the induced dipole moment due to polarization. The electric field calculation then follows a self-consistent iterative procedure, as illustrated in Fig. 3 (see the Supplemental Material [33] for details).

In this methodology, Alq_3 and DCM2 permanent dipole moments initially are distributed in a $70 \times 70 \times 70$ cubic lattice, with a lattice constant of 8.5 Å. This lattice constant is chosen in order to reproduce the same density as the amorphous Alq_3 matrix. The ratio of DCM2 and Alq_3 dipoles is selected with respect to the DCM2 concentration in the Alq_3 host. All dipole moments are randomly oriented. In the second step, we calculated the electric field at each DCM2 and Alq_3 molecule due to the random distribution of dipoles. Thus, the induced dipole moment on each molecule is obtained from the calculated polarizability tensor, and the total dipole moment is obtained as the sum of induced and permanent moments. Then the electric fields are recalculated, and the convergence criteria are analyzed. The iterative process repeats until convergence is achieved. After convergence, the DCM2 gaps are calculated using Eq. (1).

The result of this procedure is shown in Fig. 4 as a histogram showing the probability distribution of DCM2 HOMO-LUMO gaps. The DCM2 gap distribution is asymmetric, with a long tail in the low-energy region. This is a direct consequence of the nonlinearity of the Stark shifts [see Fig. 2(a)]. For energies lower than $E_0 = 2.96$ eV, the gap distribution shows a behavior that is approximately a linear combination of a Gaussian and an exponential function. For energies higher than E_0 the behavior is approximately exponential. Based on these empirical behaviors, it is possible to write an analytical expression for the probability distribution of the DCM2 gap (which will be used in Sec. IV). The expression for the probability distribution is

$$P(E_g) = \begin{cases} A\exp[\frac{-(E_g-E_0)^2}{2\sigma^2}] + B\exp[\frac{(E_g-E_0)}{\epsilon_1}] & \text{if } E_g \leqslant E_0, \\ C\exp[\frac{-(E_g-E_0)}{\epsilon_2}] & \text{if } E_g > E_0, \end{cases} \tag{2}$$

where A, B, and C are normalization constants, E_g is the DCM2 energy gap distribution, and E_0, σ, ϵ_1, and ϵ_2 are free parameters to be adjusted in order to fit the data points. Table II shows these parameters for various DCM2 concentrations.

Figure 4 shows that, surprisingly, for low DCM2 concentration the gap distribution does not depend significantly on the DCM2 concentration. Therefore, we conclude that the gap distribution is mostly determined by the random electric field produced by Alq_3 dipoles, different from the usual understanding. Although Alq_3 molecules have a smaller dipole moment, they are found more frequently near a given DCM2, thus explaining this behavior.

However, if this is the case, how can we understand the redshift due to increasing the DCM2 concentration? In Sec. IV, we present kinetic Monte Carlo simulations of exciton

TABLE II. Optimized parameters used in Eq. (2) to fit the data points shown in Fig. 4.

DCM2 concentration (%)	E_0 (eV)	ϵ_1 (eV)	ϵ_2 (eV)	σ (eV)
1	2.95944	0.10934	0.03800	0.02318
2	2.95904	0.11816	0.04500	0.02733
5	2.95605	0.12564	0.04900	0.02800
10	2.95735	0.14416	0.05100	0.03200

dynamics [34,35] performed with the purpose of answering this question.

IV. KINETIC MONTE CARLO

We propose that the emission redshift in Alq$_3$:DCM2 upon increasing DCM2 concentration is caused by diffusion and partial thermalization of excitons (limited by the exciton lifetime [36]). We propose that exciton diffusion in our system is described by FRET, which is a nonradiative energy transfer mechanism based on dipole-dipole coupling, where a donor molecule in an electronically excited state transfers its excitation energy to a nearby acceptor molecule [37]. For efficient energy transfer, it is necessary that the emission spectrum of the donor molecules overlaps the absorption spectrum of the acceptor molecules, and the separation distance between the donor and acceptor centers has to be much less than the wavelength [38].

In our model, the exciton dynamics occur through two steps:

(1) After exciton formation on an Alq$_3$ molecule (either by electric or photoexcitation), the excitation is quickly transferred to the nearest DCM2 molecule. This nonradiative energy transfer by Förster mechanism is very efficient due to good spectral overlap between the donor (Alq$_3$) emission and acceptor (DCM2) absorption spectra, shown by the yellow region in Fig. 5(a).

(2) When excitons reach DCM2 molecules or if they are initially formed directly on DCM2 molecules due to charge trapping, they can thermalize by hopping between DCM2 molecules also via the Förster process since there is a smaller but non-negligible overlap between DCM2 emission and absorption spectra [Fig. 5(b)]. Under energetic disorder, excitons move preferentially to lower-energy sites. The thermalization process lasts until they finally decay radiatively (i.e., after the exciton lifetime is reached, on average).

As stated above, the magnitude of the spectral overlap between the emission and absorption of donor and acceptor molecules is a key ingredient of the Förster mechanism. We measure these quantities, and the results are displayed in Fig. 5, which shows the experimental data for absorption and photoluminescence of an Alq$_3$:DCM2 matrix with a concentration of the guest material (DCM2) of 5% in the host material (Alq$_3$). Both molecules were purchased from Lumtec and used without additional purification. The organic film was deposited in a high-vacuum environment (10^{-6} Torr) by thermal evaporation onto a quartz substrate and with a thickness of 50 nm. The quartz substrates were cleaned by ultrasonification using a detergent solution followed by ultrasonification with deionized water, followed by pure acetone, then pure isopropyl alcohol. For the organic layers the deposition rate was 0.5 Å/s. UV-visible absorption spectra of the thin films were recorded using a Perkin-Elmer Lambda 950 dual-beam spectrometer with spectral correction. Thin-film photoluminescence spectra were measured using a PTI fluorimeter (model QuantaMaster 40) at room temperature and pressure conditions. The results in Fig. 5 show clearly the larger overlap for Alq$_3$-DCM2 with respect to DCM2-DCM2, thus justifying the larger Förster radius used in simulations (see below) for the first case.

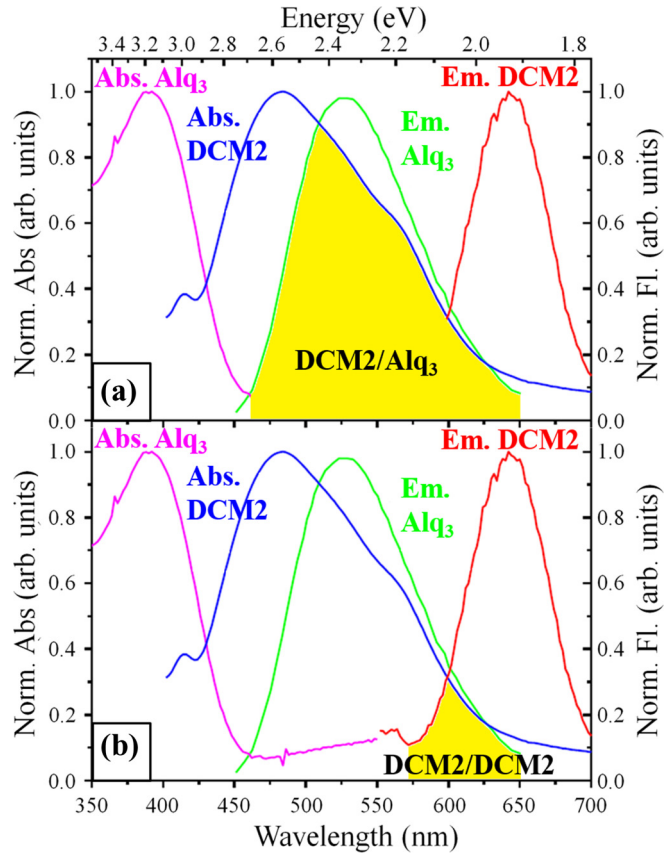

FIG. 5. Experimental absorption and photoluminescence spectra for Alq$_3$ and DCM2 in a thin film 50 nm thick, obtained in this work. (a) Overlap (highlighted yellow region) between the Alq$_3$ emission and DCM2 absorption spectra and (b) overlap (highlighted yellow region) between the emission and absorption spectra of DCM2. These overlap areas (highlighted in yellow in both panels) are associated with the Förster radius in the FRET process.

Due to the stochastic nature of the exciton hopping process, the exciton diffusion process is modeled by a kMC method based on the FRET within the first-reaction method (FRM) approximation [35,39]. The sample is modeled as a cubic lattice of $100 \times 100 \times 100$ sites, with a certain proportion of DCM2 and Alq$_3$ sites given by the dopant concentration. The lattice constant is set to 1 nm. Then, 10^4 excitons are randomly distributed in the cubic lattice, and the exciton dynamics simulation using the FRET process starts.

In the FRET model, the hopping time t_{FRET} between any two sites i and j is given by

$$t_{\mathrm{FRET}}^{ij} = t_0 \left(\frac{R_{ij}}{R_0}\right)^6 \frac{1}{f(E_i, E_j)}, \tag{3}$$

where t_0 is the exciton lifetime, R_0 is the Förster radius, and $f(E_i, E_j)$ is a function accounting for energetic disorder. The exciton lifetime t_0 is 1.0 ns. The Förster radius is proportional to the overlap between the donor (Alq$_3$) and acceptor (DCM2) emission spectra, integrated in the energy axis [see Fig. 5(a)]. As there is a smaller overlap between DCM2 emission and absorption spectra [see Fig. 5(b)], in the simulations we use two distinct R_0: one to account for the jumps between Alq$_3$ and DCM2 ($R_0 = 39$ Å) and another between DCM2-DCM2

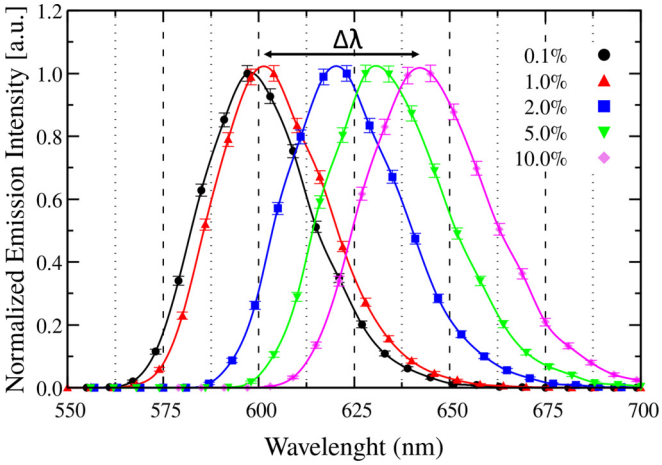

FIG. 6. Normalized emission spectra obtained from KMC simulations for various DCM2 concentrations. The plot shows a redshift from 600 to around 645 nm, $\Delta\lambda \sim 45$ nm.

molecules ($R_0 = 6$ Å). The R_0 value for Alq_3/DCM2 energy transfer was taken from the literature [10,40,41], whereas the DCM2/DCM2 value was calculated using the ratio between the two yellow areas in Fig. 5.

The function $f(E_i, E_j)$ introduces the preferential hopping of excitons to lower-energy sites and accounts for energetic disorder:

$$f(E_i, E_j) = \begin{cases} \exp[\frac{-(E_j - E_i)}{k_B T}] & \text{if } E_j > E_i, \\ 1 & \text{if } E_j \leqslant E_i. \end{cases} \quad (4)$$

The energies E_i of all Alq_3 sites are randomly assigned according to a Gaussian distribution with a standard deviation σ extracted from Gaussians fit to the Alq_3 absorption spectrum as described in Scheidler *et al.* [42]. For DCM2 sites, the energies E_i are randomly assigned according to the gap probability distribution function from Eq. (2), obtained in Sec. III.

In the FRM, a random number X between 0 and 1 is selected for each process, and a "jump time" is calculated:

$$t^{ij}_{\text{jump}} = -t^{ij}_{\text{FRET}} \ln X. \quad (5)$$

The process with the lowest jump time is then selected to be the next destination of the exciton. The jump times for each exciton are summed, and this process happens until the total event time reaches the exciton lifetime of 1 ns. When this occurs, we assume that the exciton is annihilated by emitting a photon. Then, the gap energy at the emission site is collected in a histogram (see Fig. 6). For all DCM2 molecules, the HOMO-LUMO gap energy at zero field E_0 is empirically redshifted by 0.25 eV to reproduce the emission energy of the Alq_3:DCM2 system at very low DCM2 concentrations. In order to ensure the homogeneity of the DCM2 distribution and to reduce the effects of the initial location of excitons, a total of 100 independent simulations were carried out for each concentration. Then, the final emission spectrum is obtained as the average of all spectra obtained for a given concentration of DCM2.

All this theoretical effort culminates in the emission spectra shown in Fig. 6 as a function of DCM2 concentration. As the DCM2 concentration increases, the redshift in the emission spectra is observed. An experimental $\Delta\lambda \sim 50$ nm shift from 1% to 10% DCM2 concentration is reproduced [10,11]. In addition, the bandwidth remains practically unchanged, as in experiments.

This is a very interesting result since no assumption of local aggregation of DCM2 was needed and, as shown in the previous section, the DCM2 gap distribution does not change considerably with concentration (in this low-concentration regime). Physically, we can understand the emission redshift as a consequence of the higher mobility of excitons when the DCM2 concentration increases: Within the exciton lifetime, for higher DCM2 concentrations, exciton DCM2-DCM2 jumps occur more frequently, and therefore, excitons have a better chance to thermalize to molecules with smaller gaps, thus causing an overall redshift of the average emission frequency.

V. CONCLUSIONS

In conclusion, using a combination of different theoretical methods and techniques, we proposed a mechanism for the concentration-dependent emission redshift Alq_3:DCM2 based on exciton dynamics. Our theoretical modeling was composed of several important ingredients, which we now summarize: (1) DCM2 molecules suffer a nonlinear Stark shift of the electronic gap upon external electric fields, with a negative curvature (tendency to smaller gaps). (2) When DCM2 molecules are placed in an Alq_3 matrix, the random dipole moments of neighboring molecules produce local electric fields that generate a distribution probability of DCM2 with a long tail towards low energies. For low DCM2 concentrations, these local fields are caused primarily by Alq_3 molecules, different from the usual understanding. (3) Exciton hopping from Alq_3 to DCM2 and especially between DCM2 molecules allows thermalization of excitations towards lower energies and explains the redshift. For larger concentrations of DMC2, exciton mobility is larger, and therefore, the redshift is more substantial. Our model agrees quantitatively with experiments, and we believe it describes a very general mechanism that should occur in similar systems.

ACKNOWLEDGMENTS

The authors acknowledge financial support from Brazilian agencies CNPq, FAPERJ, Finep, INCT-Nanomateriais de Carbono, and INCT-INEO for financial support. R.G. wishes to thank Dr. U. Mello, director of IBM Research-Brazil, for partial support of this project and his colleagues on the Smarter Devices team for many stimulating discussions. G.C. gratefully acknowledges FAPERJ Processo E-26/200.008/2020 for financial support. The authors wish to thank Dr. J. H. S. Restrepo from Universidad Pontificia Bolivariana, Medellin, Colombia, for providing the experimental data. The authors also acknowledge the support of Núcleo Avançado de Computação de Alto Desempenho (NACAD/COPPE/UFRJ) and Sistema Nacional de Processamento de Alto Desempenho (SINAPAD).

[1] D. D. C. Bradley, Synth. Met. **54**, 401 (1993).

[2] J. R. Sheats, H. Antoniadis, M. Hueschen, W. Leonard, J. Miller, R. Moon, D. Rottman, and A. Stocking, Science **273**, 884 (1996).

[3] F. Nüesch, D. Berner, E. Tutiš, M. Schaer, C. Ma, X. Wang, B. Zhang, and L. Zuppiroli, Adv. Funct. Mater. **15**, 323 (2005).

[4] A. Soman, A. K. Sajeev, K. Rajeev, and K. N. Narayanan Unni, ACS Omega **5**, 1698 (2020).

[5] K. T. Kamtekar, A. P. Monkman, and M. R. Bryce, Adv. Mater. **22**, 572 (2010).

[6] V. Bulović, V. B. Khalfin, G. Gu, P. E. Burrows, D. Z. Garbuzov, and S. R. Forrest, Phys. Rev. B **58**, 3730 (1998).

[7] M. Čehovski, J. Becker, O. Charfi, H.-H. Johannes, C. Müller, and W. Kowalsky, Appl. Sci. **10**, 2805 (2020).

[8] Y. Zhang and S. R. Forrest, Phys. Rev. B **84**, 241301(R) (2011).

[9] Y. Chin and L. Barbato, US Patent Application 10/737, 980 (2005).

[10] V. Bulović, A. Shoustikov, M. Baldo, E. Bose, V. Kozlov, M. Thompson, and S. Forrest, Chem. Phys. Lett. **287**, 455 (1998).

[11] C. F. Madigan and V. Bulović, Phys. Rev. Lett. **91**, 247403 (2003).

[12] M. A. Baldo, D. F. O'Brien, M. E. Thompson, and S. R. Forrest, Phys. Rev. B **60**, 14422 (1999).

[13] V. T. Förster, Ann. Phys. (Berlin, Ger.) **437**, 55 (1948).

[14] I. L. Medintz and N. Hildebrandt, *FRET-Förster Resonance Energy Transfer: From Theory to Applications* (Wiley, Hoboken, NJ, 2013).

[15] K. O. Cheon and J. Shinar, Phys. Rev. B **69**, 201306(R) (2004).

[16] X. Liu, Y. Zhang, and S. R. Forrest, Phys. Rev. B **90**, 085201 (2014).

[17] J. Becker, M. Čehovski, R. Caspary, W. Kowalsky, and C. Mueller, Microelectron. Eng. **181**, 29 (2017).

[18] C. W. Tang, S. A. VanSlyke, and C. H. Chen, J. Appl. Phys. **65**, 3610 (1989).

[19] J. Kalinowski, W. Stampor, P. Di Marco, and V. Fattori, Chem. Phys. **182**, 341 (1994).

[20] V. Bulović, R. Deshpande, M. E. Thompson, and S. R. Forrest, Chem. Phys. Lett. **308**, 317 (1999).

[21] C. Reichardt and T. Welton, *Solvents and Solvent Effects in Organic Chemistry* (Wiley, Hoboken, NJ, 2011).

[22] M. A. Baldo, Z. G. Soos, and S. R. Forrest, Chem. Phys. Lett. **347**, 297 (2001).

[23] M. J. Frisch, G. W. Trucks, H. B. Schlegel, G. E. Scuseria, M. A. Robb J. R. Cheeseman, Montgomery, Jr., J. A., T. Vreven, K. N. Kudin, J. C. Burant *et al.*, *Gaussian03, Revision C.02*, Gaussian, Inc., Wallingford, CT, 2004.

[24] J. P. Perdew, K. Burke, and M. Ernzerhof, Phys. Rev. Lett. **77**, 3865 (1996).

[25] J. P. Perdew, K. Burke, and M. Ernzerhof, Phys. Rev. Lett. **78**, 1396 (1997).

[26] C. Adamo and V. Barone, J. Chem. Phys. **110**, 6158 (1999).

[27] R. Ditchfield, W. J. Hehre, and J. A. Pople, J. Chem. Phys. **54**, 724 (1971).

[28] A. D. Becke, Phys. Rev. A **38**, 3098 (1988).

[29] C. Lee, W. Yang, and R. G. Parr, Phys. Rev. B **37**, 785 (1988).

[30] K. Kim and K. Jordan, J. Phys. Chem. **98**, 10089 (1994).

[31] P. J. Stephens, F. Devlin, C. Chabalowski, and M. J. Frisch, J. Phys. Chem. **98**, 11623 (1994).

[32] A. Curioni, M. Boero, and W. Andreoni, Chem. Phys. Lett. **294**, 263 (1998).

[33] See Supplemental Material at http://link.aps.org/supplemental/10.1103/PhysRevB.102.235401 for details of the methods used in this paper.

[34] F. Fennel and S. Lochbrunner, Phys. Rev. B **85**, 094203 (2012).

[35] C. Madigan and V. Bulović, Phys. Rev. Lett. **96**, 046404 (2006).

[36] L. M. Herz, C. Silva, A. C. Grimsdale, K. Müllen, and R. T. Phillips, Phys. Rev. B **70**, 165207 (2004).

[37] M. Lunz, A. L. Bradley, V. A. Gerard, S. J. Byrne, Y. K. Gun'ko, V. Lesnyak, and N. Gaponik, Phys. Rev. B **83**, 115423 (2011).

[38] J. Ren, T. Wu, B. Yang, and X. Zhang, Phys. Rev. B **94**, 125416 (2016).

[39] K. Feron, X. Zhou, W. J. Belcher, and P. C. Dastoor, J. Appl. Phys. **111**, 044510 (2012).

[40] R. Deshpande, V. Bulović, and S. Forrest, Appl. Phys. Lett. **75**, 888 (1999).

[41] M. A. Baldo, M. E. Thompson, and S. R. Forrest, Nature (London) **403**, 750 (2000).

[42] M. Scheidler, U. Lemmer, R. Kersting, S. Karg, W. Riess, B. Cleve, R. F. Mahrt, H. Kurz, H. Bässler, E. O. Göbel, and P. Thomas, Phys. Rev. B **54**, 5536 (1996).